

Mesoscale modelling of concrete for static and dynamic response analysis Part 2: numerical investigations

Yong Lu*¹ and Zhenguo Tu²

¹*Institute for Infrastructure and Environment, Joint Research Institute for Civil and Environmental Engineering, School of Engineering, The University of Edinburgh, EH9 3JL, UK*
²*IKM Ocean Design As, Vassbotnen 1, 4313 Sandnes, Norway*

(Received October 19, 2009, Accepted September 27, 2010)

Abstract. As a brittle and heterogeneous material, concrete behaves differently under different stress conditions and its bulk strength is loading rate dependent. To a large extent, the varying behavioural properties of concrete can be explained by the mechanical failure processes at a mesoscopic level. The development of a computational mesoscale model in a general finite element environment, as presented in the preceding companion paper (Part 1), makes it possible to investigate into the underlying mechanisms governing the bulk-scale behaviour of concrete under a variety of loading conditions and to characterise the variation in quantitative terms. In this paper, we first present a series of parametric studies on the behaviour of concrete material under quasi-static compression and tension conditions. The loading-face friction effect, the possible influences of the non-homogeneity within the mortar and ITZ phases, and the effect of randomness of coarse aggregates are examined. The mesoscale model is then applied to analyze the dynamic behaviour of concrete under high rate loading conditions. The potential contribution of the mesoscopic heterogeneity towards the generally recognized rate enhancement of the material compressive strength is discussed.

Keywords: concrete mesoscopic heterogeneity; mesoscale model; nonlinear FE analysis; quasi-static load; dynamic load; mesoscopic failure mechanism.

1. Introduction

In the companion paper (Tu and Lu 2011), a comprehensive computational mesoscale model of concrete has been presented. The model is suited for implementation in general-purpose FE platforms, and hence can be applied for analysis under a variety of stress and loading conditions.

On top of the generation of the mesoscale geometry and the finite element meshing, particular considerations are given to the modelling of the interfacial transition zone (ITZ) between aggregates and mortar matrix. Two different approaches have been examined, namely a zero-thickness interface element approach and an equivalent layer of solid element approach. It has been shown that the equivalent layer scheme provides a viable alternative for modelling the ITZ. To tackle the numerical

*Corresponding author, Professor, E-mail: yong.lu@ed.ac.uk

difficulties that tend to arise due to localized high nonlinearity and material softening during the failure process, an explicit scheme is adopted for both quasi-static and dynamic loading conditions.

This paper presents a series of numerical investigations using the above mesoscale model into the concrete behaviour under both quasi-static and dynamic conditions. The basic mesoscale mechanisms involved in the damage and failure under uniaxial compression and tension are examined. Parameters being investigated include the lateral confinement due to friction at the loading faces, non-homogeneity of material distribution within the mortar and ITZ phases, and the randomness of geometry of the coarse aggregates. Results will highlight the importance of a realistic incorporation of the ITZ into the numerical model in order to achieve a satisfactory prediction of the concrete behaviour. It will also be shown that the uncertainty in the experimentally observed concrete strength is mainly attributable to the friction condition at the loading faces, while the non-homogeneity at the sub-mesoscale level, i.e., within the mortar and ITZ phases, play a less significant role.

In the last part of the paper, the mesoscale model is further applied to investigate the rate-dependent behaviour of concrete under dynamic loading conditions. In particular, the contribution of the material heterogeneity towards the experimentally observed rate enhancement of the concrete compressive strength is evaluated based on the simulations with four different model considerations. The variation of concrete fracture modes at different strain rates and its implication on the bulk dynamic strength enhancement is also discussed.

2. Basic numerical model configurations

For simplicity and without losing generality concerning the characteristics of the underlying mechanisms, all the analyses are conducted for a representative class of concrete with a nominal compressive strength of 30 MPa. The coarse aggregates have a size range of 5-20 mm, and the volumetric ratio of coarse aggregates is 40%, which is typical for normal strength concrete.

The material properties used in the model for mortar, ITZ and coarse aggregates for the 30 MPa concrete are determined based on data collected from relevant literature (e.g., Nagai *et al.* 2005, Bazant and Pfeiffer 1987, Agioutantis *et al.* 2000), and they are summarized in Table 1. It should be noted that the properties of mortar and ITZ listed in the table represent the mean values. When a non-uniform distribution of the material properties is considered, as will be discussed in Section 3.2, a normal probabilistic distribution will be considered with the mean equal to these values.

A standard concrete specimen of dimension $150 \times 150 \times 150$ mm, as usually used in the laboratory test of concrete, is considered. The specimen is modelled in a 2D plane stress condition.

Table 1 Properties of concrete constituent materials

Properties	Mortar	ITZ	Aggregate
Elastic modulus (GPa)	22	19	60
Poisson's ratio	0.2	0.2	0.2
Density (kg/m ³)	2000	2000 (equivalent ITZ)	2600
Compressive strength (MPa)	35	26.25	
Tensile strength (MPa)	3.48	2.6	
Fracture energy (N/m)	42	30	

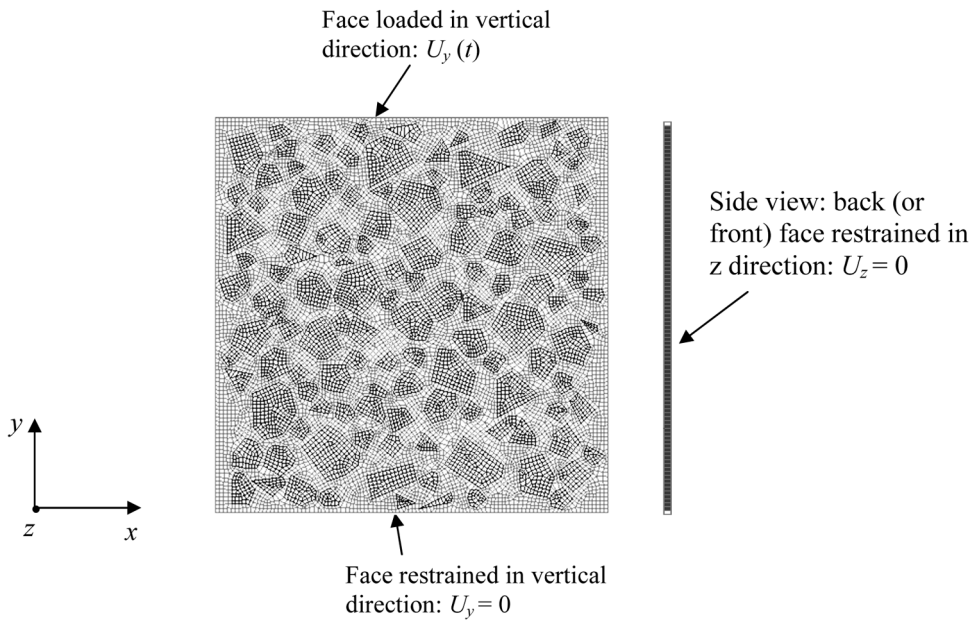


Fig. 1 Mesoscale FE model configuration

The configuration of the specimen and a sample mesoscale FE model is shown in Fig. 1. To simulate the uniaxial loading condition, the specimen is fixed at the bottom face and loaded from the top edge in the Y direction. In order to be able to produce the full range of the concrete response including the softening stage, the loading is applied in a displacement-controlled mode through imposing a velocity boundary condition.

It is noted that all uniaxial compression simulations are conducted without loading face friction, except for the analysis in which the friction confinement effect is specifically included for a comparison, as will be discussed in Section 3.1. The idealized friction-free condition resembles a true uniaxial external loading condition. It actually represents a lower bound scenario in actual concrete tests, and as such the simulated results will tend to be at the lower end when comparing to general experimental observations for the same class of concrete.

As explained in the companion paper (Tu and Lu 2011), the 2D mesoscale model is put in a thin-plate configuration so as to allow the use of solid elements, with a single layer of elements in the out-of-plane direction. A nominal thickness of 1.0 mm is used, which is consistent with the mesh grid size in the 2D plane. To ensure that the model responds only in the 2D plane, the out-of-plane constraints are imposed on the back (or front) surface in a plane stress simulation. It is worthy mentioning that, when both front and back surfaces are restrained from out-of-plane movement, the model will resemble a plane strain condition.

Loading is achieved by applying a velocity boundary condition following a gradually increased velocity pattern. A rise time of 4 ms in conjunction with a flat velocity of 0.05 m/s are found to be appropriate for the compression analyses. These values need to be adjusted for analysis under other loading conditions, as will be explained in the respective sections later. All the analyses are performed using the transient dynamic solver LS-DYNA (2007).

3. Mesoscale investigation of concrete under uniaxial quasi-static compression

Generally speaking, the behaviour of concrete may be characterized by the strength, stress softening and the failure mode. In practice, these behavioural parameters are determined by testing control concrete specimens. It is commonly known that even for the same batch of concrete mix, an appreciable level of scatter usually occurs in the test results. Such a scatter may be attributed to several uncertainties, including chiefly a) the non-homogeneity in the mortar matrix and the ITZ, b) the randomness in the detailed geometric distribution of the coarse aggregates in individual samples, c) the loading device dependent factors, particularly the friction on the loading faces, and d) the non-uniformity of the workmanship.

Whereas the workmanship is a difficult subject to model, other factors may be simulated fairly realistically using the current mesoscale model. This section presents a numerical parametric investigation into the extent to which these uncertainties might affect the behaviour of concrete under compression. In addition, the general effect of variable ITZ strength on the overall concrete behaviour is also examined.

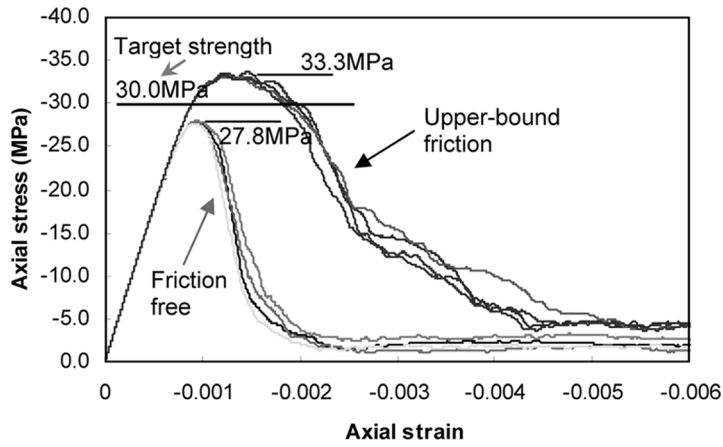
3.1 Loading-face friction effect: a validation study

The loading-face friction effect on the compressive behaviour of a concrete specimen is widely observed and well documented in the literature. This effect is examined in this section using the present mesoscale model, which also serves as a basic validation of the model against relevant experimental observations.

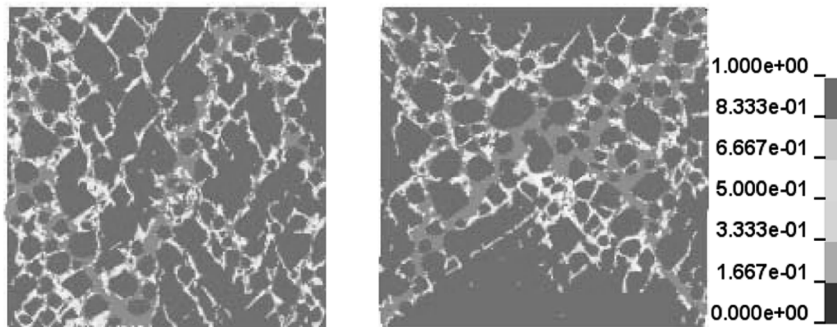
In the current mesoscale model, it is possible to simulate the varying friction forces applied on the loading faces by incorporating friction springs. For simplicity, only two borderline scenarios are considered herein, one is friction free (lower bound scenario), and another with a complete lateral constraint on the top and bottom faces (upper bound scenario). A typical laboratory test with a standard steel loading piston should fall in-between the above two extreme situations.

A number of comparative simulations are conducted, using several mesoscale models with randomly sampled aggregate structures. Each sample model is subjected to axial compression with the above-mentioned upper and lower friction effects, respectively. The computed axial stress-strain curves and typical failure patterns are shown in Fig. 2(a)-(b). Note that the axial stress is evaluated as the total nodal forces in the axial direction on the loading face divided by the loading area. A set of representative experimental results from the literature (van Vliet and van Mier 1996) are shown in Fig. 2(c) for a comparison. It should be noted that the concrete used in experiment had a higher strength (~40 MPa) than that in the numerical models (~30 MPa), and this should be taken into account when comparing the absolute results.

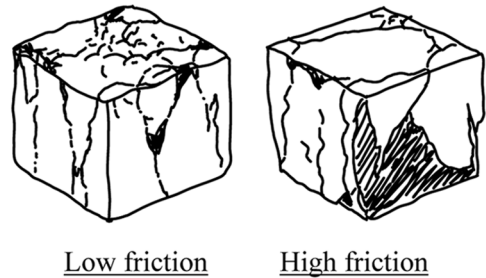
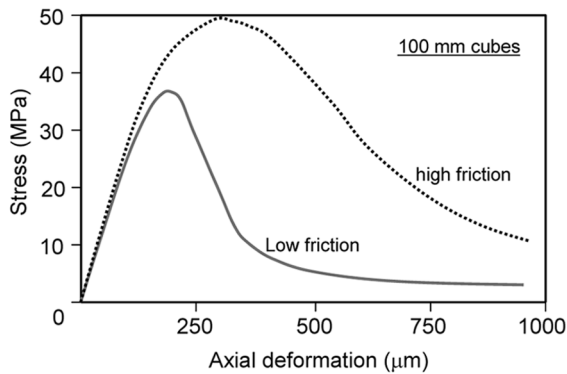
As can be seen, both the strength and the ductility (softening response) show significant enhancement due to the presence of the friction confinement on the loading faces, and in this regard the numerical and experimental results agree very well. In the numerical results, the concrete strength increases on average from 27.8 MPa without friction to 33.3 MPa under the upper bound friction, i.e., an increase of about 20%. If we take the average between the two bound values as a reasonable representation of the strength under a normal device-induced friction condition, it gives a strength about 30 MPa, which is very close to the target nominal strength of 30 MPa that the mesoscale model aims to achieve. If we further treat the upper and lower bound strengths as extreme values in the context of a normal distribution (e.g., 3 times the standard deviation), it would



(a) Computed compressive stress-strain curves with different boundary friction conditions



(b) Computed failure patterns: left = friction free, right = upper-bound friction (Colour scale: 1.0 = total damage)



(c) Typical experimental results (after van Vliet and van Mier 1996)

Fig. 2 Mesoscale simulation results under quasi-static compression and comparison with typical experimental observations

lead to a coefficient of variance (COV) around 3% that can be attributed to the device-induced friction effect.

From the computed fracture patterns, it can be clearly observed that the presence of the friction confinement on the loading faces also changes the characteristic of the compression failure mode, i.e., from an inclined crack mode to an apparent double-cone pattern. This observation also agrees favourably with general experimental results, as illustrated in Fig. 2(c).

3.2 Influence of non-homogeneity of mortar and ITZ

From a mesoscopic perspective the heterogeneity of concrete has three distinctive phases, i.e., aggregates, mortar matrix and the ITZ. These three phases are explicitly represented in the current mesoscale model. The materials within each phase are considered as homogeneous, although in reality these individual phases, especially mortar and the associated ITZ, are also heterogeneous. Being a sub-mesoscale feature, the non-homogeneous properties within individual phases are expected to play a less significant role in determining the bulk behaviour of concrete. However, it would be interesting to draw a clear picture as to what extent and in which aspects the bulk-scale concrete response may be affected by the non-homogeneity within mortar and ITZ phases. Such information is both computationally and physically meaningful.

To simulate the non-homogeneous properties within mortar and ITZ in a mesoscale model, the present study adopts an equivalent approach by considering a random distribution of the material properties among the FE elements for the mortar and ITZ parts, respectively. This approach is implemented as follows.

A probability density function (PDF) is first chosen to describe the distribution of the material property. Here we use the Gaussian distribution as an example, considering a mean property μ and a standard deviation σ . In the numerical implementation, the continuous probability density curve is discretized into N segments, resulting in N groups of the material, each has a mean property of S_i and a group probability of P_i . Extreme values below $\mu - 3\sigma$ or above $\mu + 3\sigma$ are combined into two end groups, respectively. In the FE model implementation, N types of material are defined for the mortar (similarly for ITZ) phase in accordance with the above grouping. Subsequently, each mortar element is assigned to one of these mortar material groups through a random sampling procedure.

The mortar material generally has better homogeneity as compared to ITZ. The coefficient of variance (COV) associated with the measured strength of mortar under a well-controlled mixing process is on the order of 5% (Mindess and Young 2003). The ITZ material is more difficult to characterise, but it tends to be accepted that in a typical situation the strength of ITZ is around half of that of the mortar matrix (Agioutantis *et al.* 2000). No specific data is available about the COV associated with the ITZ properties except the general understanding that it is much higher than that of mortar. For this reason, the COV for the ITZ material is assumed to be 20% in the present study, representing a fairly high level of uncertainty.

Fig. 3 shows samples of stochastic spatial material distributions in mortar and ITZ, respectively. In the figure, elements in different colours (or darkness) indicate different material properties within the same phases.

In order to evaluate the influence of the non-homogeneity in mortar and ITZ respectively, two separate sets of simulations are performed, each having one of the two phases following a stochastic distribution while the other phase maintaining a uniform (mean) property. The loading faces of the specimen are considered free of friction to avoid complications from other factors.

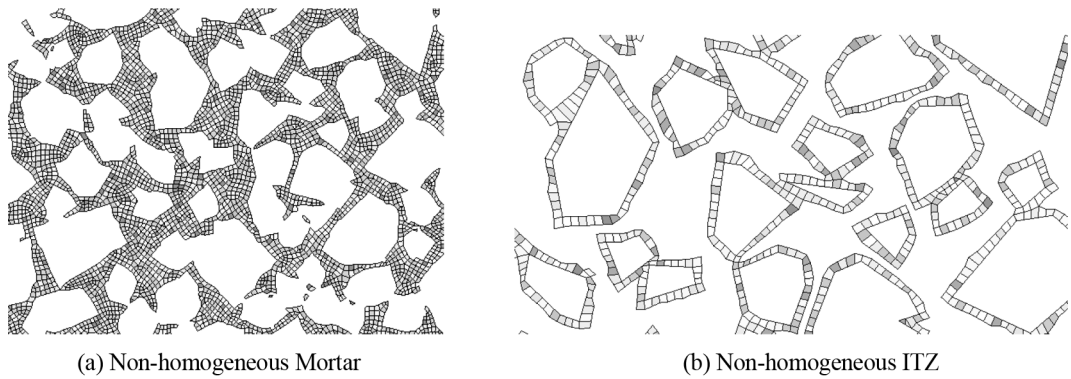
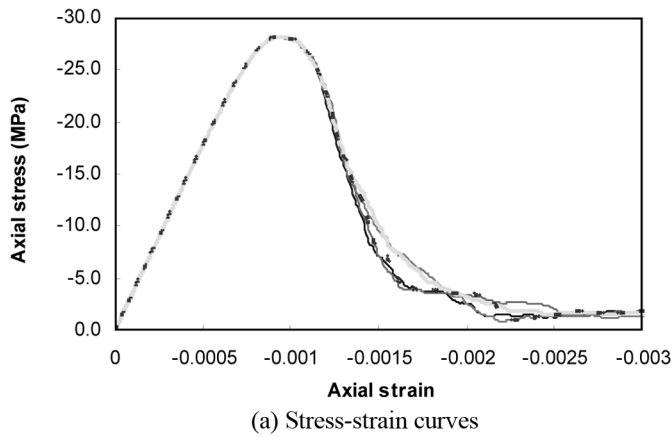
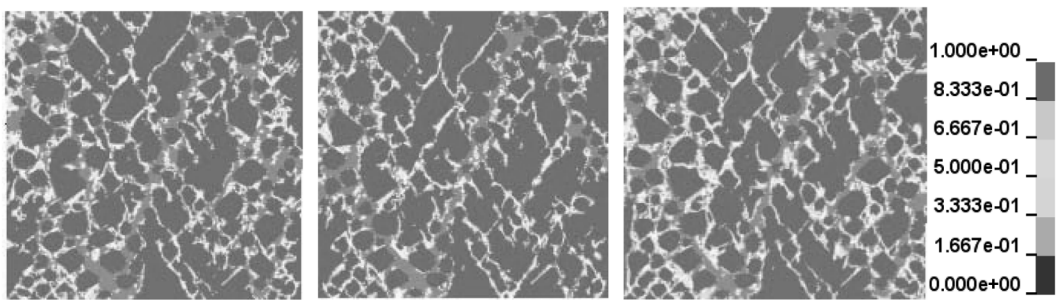


Fig. 3 Representation of non-homogeneous material distribution in mortar and ITZ (Note: different colours or darkness represents different groups of material properties)



(a) Stress-strain curves



(b) Typical failure patterns

Fig. 4 Simulation results under uniaxial compression using mesoscale model with non-homogeneous distributions of mortar properties (Colour scale: 1.0 = total damage)

3.2.1 Influence of non-homogeneity in mortar matrix on the concrete response

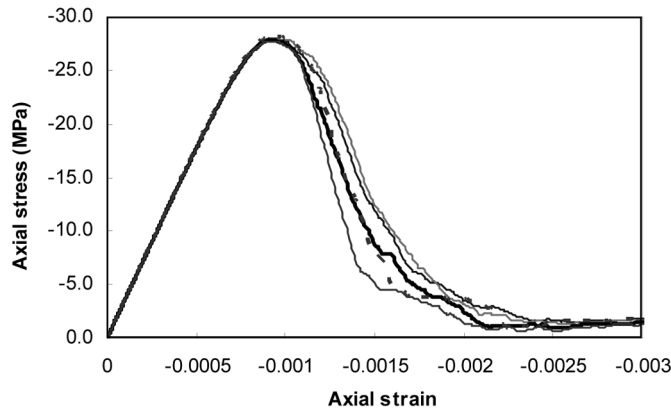
Ten samples of the mesoscale model are created for this evaluation. All samples have the same overall mesoscale model setting, but vary in the detailed spatial distribution of the mortar properties as a result of random sampling from the same probability distribution of mortar.

Fig. 4(a) shows the typical compressive stress-strain curves produced from different samples, together with that with homogenous mortar and ITZ (dashed line). It can be seen that the results are almost identical except some differences at the tail part of the curves, which essentially have no practical significance. This indicates that the non-homogeneity within the mortar matrix has little effect on the bulk behaviour of concrete.

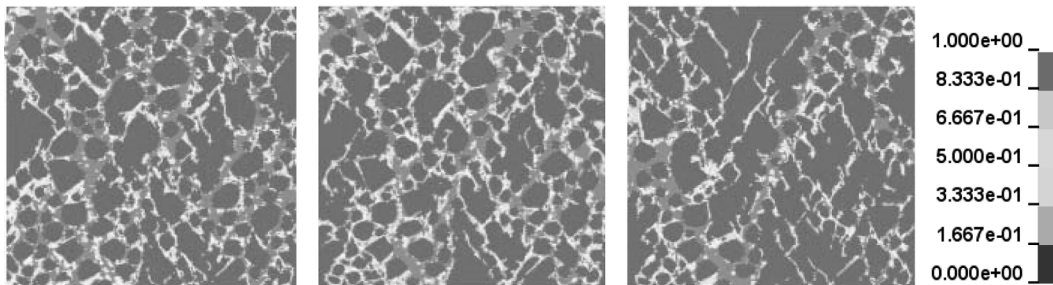
Representative failure modes from different samples are depicted in Fig. 4(b). The overall failure pattern is similar, although some difference exists in the local distribution of the damage within the mortar matrix, as can be expected as a result of the variation in the distribution of the mortar properties in different models. The primary failure pattern is dominated by a few major fracture lines in inclined vertical directions, along with secondary fracture lines running in a similar pattern. This agrees well with the experimental observations for compressive specimens with low friction confinement on the loading faces (Fig. 2(a)).

3.2.2 Influence of non-homogeneity in ITZ on the concrete response

Following a similar procedure, the effect of the non-homogeneous distribution of properties within the ITZ elements is simulated. Fig. 5(a) depicts the stress-strain results obtained by a few models having the same general mesoscale structure and uniform mortar property but randomly sampled properties within the ITZ elements. The result from the model in which both mortar and ITZ are



(a) Stress-strain curves



(b) Typical failure patterns (Colour scale: 1.0 = total damage)

Fig. 5 Simulation results under uniaxial compression using mesoscale model with non-homogeneous distributions of ITZ properties

considered as homogeneous is also included (dashed line). The variation in the failure patterns is illustrated in Fig. 5(b).

Similar to the observations made from the analysis with random mortar properties, the influence of the uncertainty within the ITZ has little effect on the elastic and the peak strength of the concrete specimen. However, the variation in the softening stage among different sample models becomes more pronounced as compared to Fig. 4(a). This is clearly attributable to the larger variation (COV = 0.2) in the probabilistic distribution of the ITZ properties, resulting in a larger variation in the fracture paths among the different sample models, as evidenced by the detailed failure patterns shown in Fig. 5(b). The computed stress-strain curve with both homogeneous mortar and ITZ lies at about the average of non-homogeneous samples.

The reason that the predicted strength of the concrete is not markedly affected by the uncertainty in the mortar matrix or the ITZ may be explained by the fact that the peak stress is determined by the formation of a few dominant macrocracks. These macrocracks do not differ characteristically for the sample specimens with the same overall mesoscale structure. However, the uncertainties within the mortar and ITZ affect the detailed fracture distributions, and consequently influence the softening stage of the response in a more sensible manner.

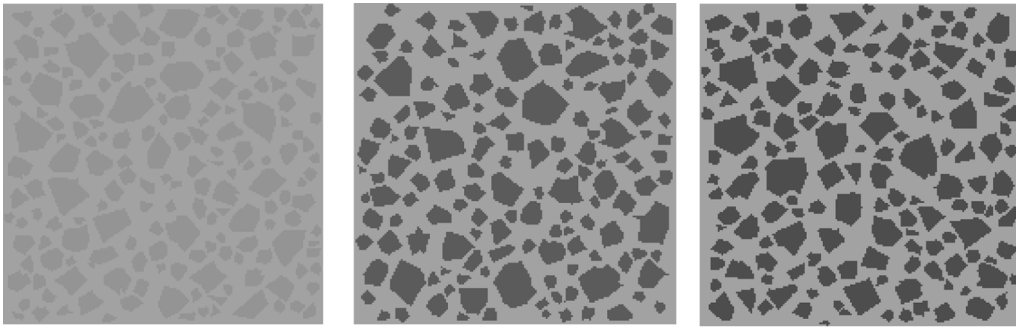
3.3 Influence of random aggregate structure

Coarse aggregates are the main source of heterogeneity in concrete. For the same concrete mix using the same batch of aggregates, different sample specimens may be considered as having the same composition of aggregates from a statistical point of view. However, at the mesoscopic level each individual specimen has a unique aggregate structure. The variation in the detailed aggregate structure could be a contributor to the observed uncertainty in the bulk concrete behaviour.

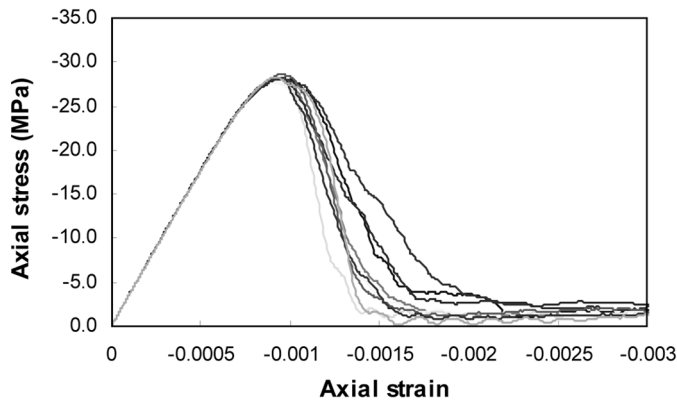
In the current mesoscale modelling framework, the variation in the detailed aggregate structure can be readily simulated by creating different samples of the mesoscale geometry for the specimen. The same aggregate grading (Fuller) curve is followed, but each complete round of sampling procedure will result in a unique mesoscale structure of aggregates, and this resembles very well the physical process of casting individual specimens from the same batch of concrete.

To evaluate the influence of the mesoscale aggregate structure on the uncertainty in the concrete response, ten sampled mesoscale models are generated with different aggregate details. Fig. 6(a) shows three typical examples. To concentrate on the influence of the aggregate structure, the mortar and ITZ phases are assumed to be homogeneous within their respective domains and have the mean material properties in all these models.

All the ten models are analyzed under a quasi-static uniaxial compression. Fig. 6(b) compares the stress-strain curves obtained from these simulations. A quite marked variation in the softening stage of the response can be observed. Comparing to the results shown in Fig. 5(a), the influence of the uncertainty in the aggregate structure on the descending branch appears to be larger than the influence due to the uncertainty associated with the ITZ. The peak stress also exhibits some noticeable variation here, and in terms of the coefficient of variance (COV) it is around 1.0% for an average strength of about 28 MPa. Therefore, this uncertainty is deemed to play a non-negligible role in the generally observed uncertainty in the compressive strength of actual concrete, which has a COV on the order 5.0% (Mindess and Young 2003) for the same batch of concrete.



(a) Typical samples of aggregate distribution (overall specimen size 150 x 150mm)



(b) Stress-strain curves

Fig. 6 Different samples of aggregate distribution and simulated compression stress-strain curves

3.4 Additional comments on the consideration of ITZ in a mesoscale model

Although the physical existence of ITZ is generally recognized, there is no specific information regarding the extent to which inaccuracy might be introduced by a simplified treatment of ignoring ITZ in a mesoscale numerical model of concrete. In some published works involving mesoscale modelling of concrete, the ITZ phase was simply ignored and the aggregates were considered to be perfectly embedded in the mortar matrix (e.g., Eckardt *et al.* 2004).

In the present mesoscale model with an equivalent layer of ITZ, a comparison can be easily made by simply assigning the normal mortar properties to the ITZ elements, thus eliminating the effect of ITZ. It may be appropriate to recall here that in the present mesoscale model for 30 MPa concrete, the mortar material is assumed to have a compressive strength of 35 MPa, whereas the equivalent ITZ has a compressive strength of about 27 MPa.

Fig. 7 shows a comparison of the compressive stress-strain curves between the models with and without considering the ITZ, for the lower and upper bound friction conditions, respectively. It can be observed that, without considering the weaker ITZ, an overestimation of the concrete strength by 10-15% could result under both friction conditions, although the overall stress-strain curves are not affected significantly.

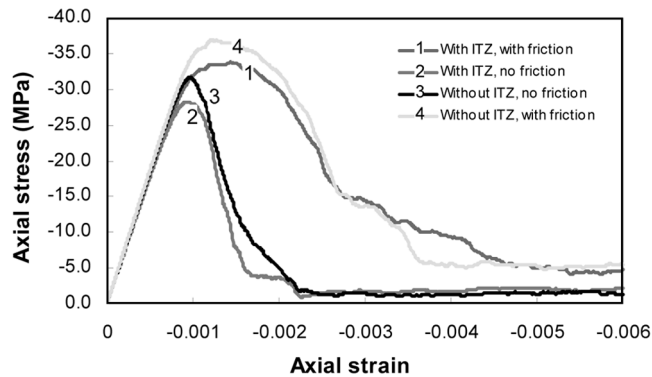


Fig. 7 Comparison of stress-strain curves from models with and without consideration of ITZ

4. Mesoscale investigation of concrete under uniaxial quasi-static tension

In this section, the mesoscale model will be used to analyze the behaviour of concrete under uniaxial tension. For concrete with a nominal compressive strength of 30 MPa under consideration, the direct tensile strength is expected to be around 2.5 MPa.

4.1 Additional modelling considerations

The basic mesoscale model configuration is the same as that created for the compression analysis. Because of the relative insignificance of the sub-scale non-homogeneity within the mortar and ITZ phases, in the tension analyses the mortar and ITZ are considered to be homogeneous within their respective domains.

Trial analyses indicate that the hourglass control settings used in the compression study are also adequate for the tension analysis. In fact, the calculated stress softening response under tension is rather insensitive to the choice of Q_{hg} . This is understandable because failure of concrete in direct tension involves only a small fraction of the material in localized regions; therefore the number of elements that might develop into an hourglass mode, and hence activate the artificial hourglass force, is limited.

Regarding the velocity loading history, the same rise curve and rise time as in the compression analysis is employed, with however the maximum velocity being reduced to 0.003 m/s, i.e. about 10% of the velocity used in the compression analysis. This is consistent with the ratio of tensile failure strength to compressive strength.

4.2 Results and discussion

A typical simulated fracture process of concrete under uniaxial tension is depicted in Fig. 8(a). The corresponding tensile stress-strain curve is given in Fig. 8(b).

It can be observed that upon the peak stress, many micro-cracks have developed and are located mostly in the mortar-aggregate interface zones. As the strain increases, concentrated macro cracks start to emerge, and this brings the specimen into the softening stage. Because of the stress relief, unloading and recovery of the elastic deformation takes place in areas outside the strain

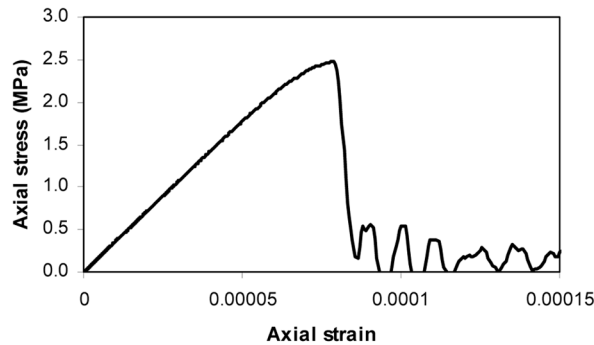
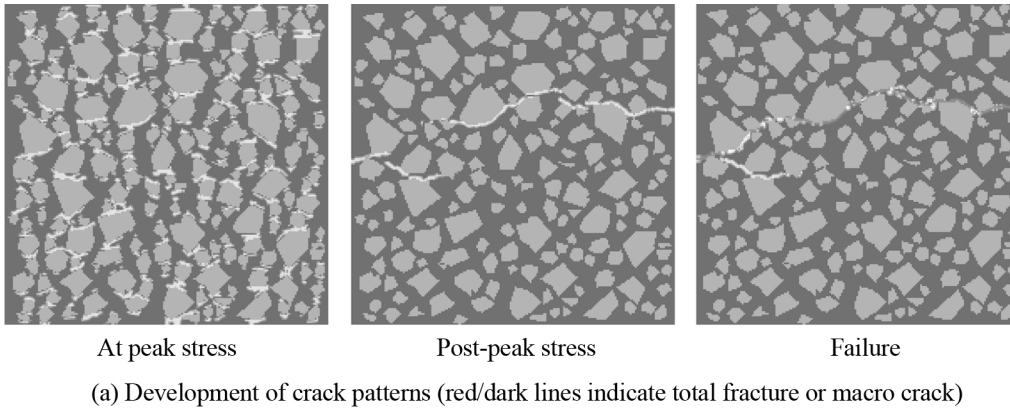


Fig. 8 Typical simulation results under uniaxial tension

localization regions. Many small micro-cracks developed earlier stop opening further. As the applied tension deformation further increases, the concentrated macro cracks propagate transversely, cutting through the mortar-aggregate interface regions, and eventually coalesce to form virtually a single major crack across the entire width of the specimen. The entire simulated fracture process is in good agreement with experimental observations (Gopalaratnam and Shah 1985, Ueda *et al.* 1993).

The localized nature of the concrete fracture under tension can result in different nominal (engineering) strain measures using different gauge lengths. Fig. 9(a) shows three different gauge lengths, namely, AA, BB and CC. The corresponding average stress-strain responses are depicted in Fig. 9(b). It becomes immediately clear that, while in the pre-peak regime the nominal strain is almost independent of the gauge length, the nominal strain in the post-peak regime (cracking stage) decreases almost proportionately as the gauge length increases. This is a characteristic of the widely known strain localization and it renders the engineering stress-strain relationship under tension to be strongly size dependent.

A pair of comparative simulations is also conducted to examine the significance of considering a weaker ITZ in the simulated tensile behaviour of concrete. As expected, if the ITZ is ignored an overestimation of the nominal tensile strength will result, and in the present case it would be 3.4 MPa as compared to about 2.5 MPa from the simulation considering ITZ.

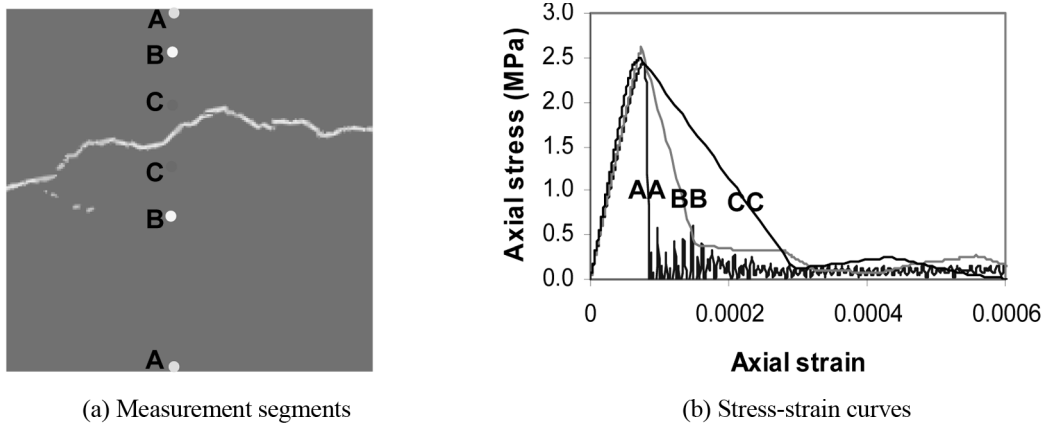


Fig. 9 Illustration of different stress-strain softening response for segments of different lengths

5. Mesoscale modelling of dynamic behaviour of concrete under compression at high strain rate

Under dynamic conditions, the nominal bulk strength of concrete is known to be rate-dependent and generally increases with the increase of the strain rate. Numerous studies have been published regarding the dynamic increase factor (DIF, defined as the ratio of the dynamic strength to quasi-static strength) of concrete strength (e.g., Tedesco *et al.* 1994, Grote *et al.* 2001, Park *et al.* 2001). However, because of various uncertain and device-dependent factors, how to best interpret the experimental DIF data and appropriately incorporate such data into a computational model remain to be a subject of continuous study (Li and Meng 2003, Dong *et al.* 2006, Zhou and Hao 2008).

One potential influencing factor on the DIF is the inherent heterogeneity in the concrete material. The mesoscale model proposed in the present study and its associated capability in accommodating a dynamic analysis makes it possible to carry out an investigation into the heterogeneity influence by means of numerical simulations. The results could also provide additional information with regard to the extent the overall DIF may be attributed to the dynamic structural effects (e.g., axial and lateral inertia) and to the underlying material mechanisms. A complete treatment of this topic will be presented elsewhere. An outline of the simulations for concrete specimens under high rate compression and a summary of the preliminary findings are given below.

For the purpose of a direct comparison, two pairs of models for the same 150-mm specimen are set up and analyzed. The first pair consists of a mesoscale model and a homogenized FE model, and in both models no rate enhancement (DIF) is considered at the constituent material level (i.e., the material properties are not rate-sensitive). This allows for an observation on the non-constitutive factors, especially the mesoscopic heterogeneity, might contribute in the dynamic enhancement of the overall specimen strength. These two models are designated as “Meso-NDIF” and “Macro-NDIF”, respectively. The second pair consists of the same meso-scale and homogenised FE models as in the first pair, but with consideration of an “embedded” DIF in the respective material models. This way of modelling the DIF is commonly adopted in the analysis of concrete structures under high rate loading, and therefore the results and their comparison with the first pair of models will provide a useful benchmark for applications using similar models. The two models in the second

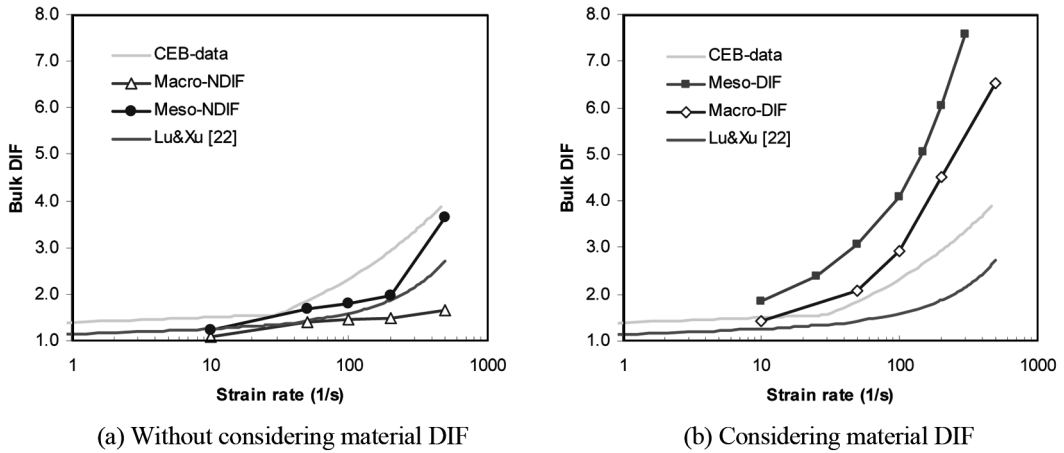


Fig. 10 Comparison of the DIF curves generated using different numerical models with empirical curves

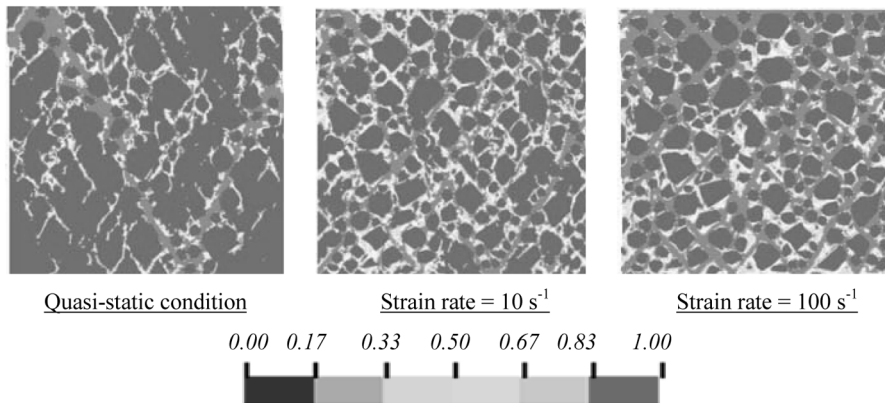
pair are designated as “Meso-DIF” and “Macro-DIF”, respectively.

The dynamic loading is simulated by applying a velocity boundary condition in a similar way as in the quasi-static analysis, but with a fast rate and a different time history in order to achieve a desirable strain rate and stress distributions. Note that in the dynamic simulations herein, no friction induced lateral confinement is considered at the loading faces.

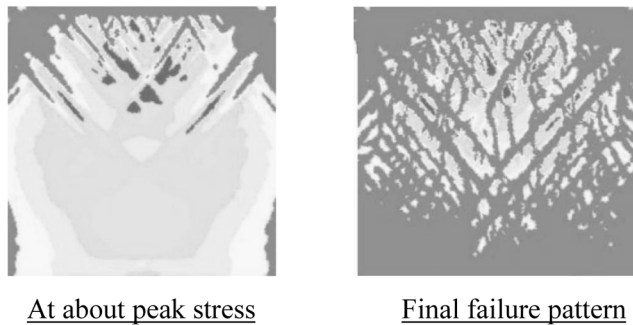
Each of the four models is analyzed for a series of loading histories corresponding to different levels of strain rate. From the results of each simulation, the bulk dynamic compressive strength is evaluated based on the total force developed at the loading face. This is consistent with the two-wave analysis method used in processing the physical test data (ASM 2000) for the same purpose.

Fig. 10 shows the variation of the predicted DIF with the strain rate from the simulations using the four different models. Shown in the figure are also the widely used CEB-FIP DIF curve for concrete (CEB 1993), and a semi-empirical curve obtained in (Lu and Xu 2004) for a comparison. The following general observations may be made:

- 1) For the two models in which no DIF is pre-imposed at the material property level, the overall dynamic strength of the specimens still exhibits significant rate enhancement in the high strain rate regime (more so for strain rate $> 100 \text{ s}^{-1}$), especially for mesoscale model “Meso-NDIF”. While the bulk DIF from the Macro-NDIF model represents primarily the dynamic inertia (axial and lateral) effects, the marked increase of the bulk DIF in the Meso-NDIF model as compared to the Macro-NDIF model highlights that the material heterogeneity plays an important role in the dynamic enhancement of the apparent compressive strength of concrete. A similar observation was also made by Zhou and Hao (2008), where a much simplified mesoscale model was employed.
- 2) The DIF obtained from the mesoscale model Meso-NDIF lies in-between the two benchmark curves, and this tends to indicate that the dynamic enhancement effects are fairly well accounted for in such a model, where both the dynamic inertia effect and the mesoscale mechanisms are represented.
- 3) On the other hand, when the full CEB-FIP DIF is imposed as a property of the constituent materials, as in the case of models “Meso-DIF” and “Macro-DIF”, the bulk dynamic strength of the specimen is consistently over-estimated.



(a) Failure patterns of the mesoscale model under different loading rates (Colour scale: 1.0 = total damage)



(b) Failure pattern of homogeneous model under compressive strain rate of 100 s^{-1}

Fig. 11 Comparison of computed failure patterns

From a mesoscopic point of view, the effect of the material heterogeneity on the dynamic strength of the bulk concrete material may be attributable to the alteration of the fracture patterns with the increase of the strain rate, as can be seen from Fig. 11 for model Meso-NDIF as compared to the homogeneous model. From a mesoscopic point of view, when the loading (strain) rate is low, there is ample time for fracture to trace the weakest path, such that the failure is dominated by a few concentrated major cracks. On the other hand, when the loading rate is very high, an effective stress re-distribution is inhibited and so damage occurs virtually everywhere within the mortar and ITZ as the stress wave propagates and the stress magnitude builds up. The involvement of higher strength paths within the specimen in the energy dissipation process gives rise to an increased resistance, which manifests at the bulk scale level as a dynamic enhancement effect. Such mesoscopic characteristics cannot be represented in a homogenized model as shown in Fig. 11(b).

6. Conclusions

In this paper, the mesoscale model presented in the companion paper is applied to investigate the

behaviour of concrete under quasi-static and dynamic stress conditions. Several factors that could potentially contribute in defining the underlying mechanisms are examined, namely, the presence of ITZ; the material non-homogeneity within the mortar and ITZ phases; the randomness of the aggregate distributions; and the friction-induced confinement at the loading faces. The effect of the mesoscopic heterogeneity on the dynamic strength enhancement of concrete is also discussed through comparative simulations.

Under compression, the friction-induced confinement at the loading faces is found to influence significantly both the failure strength and the failure modes. The failure strength corresponding to the upper bound friction confinement, i.e., with fully constrained lateral movement at the loading faces increases by about 20% as compared to the lower bound case without the friction effect.

The non-homogeneous distribution of material properties at the sub-mesoscale level, i.e., within the mortar and ITZ, does not appear to affect the behaviour of the concrete specimens in a sensible manner. The randomness in the aggregate distribution, however, has an appreciable effect on the behaviour of concrete, introducing a variation of the concrete failure strength in terms of COV at around 1.0%. The softening branch appears to be relatively more susceptible to the randomness in the subscale material non-homogeneity and the aggregate distributions.

The presence of ITZ is shown to play a significant role in determining the failure strength of concrete. With an equivalent layer of weaker elements for the ITZ, the mesoscale model reasonably reproduces the anticipated concrete strength; on the other hand, neglecting the ITZ can lead to an overestimation of the strength by more than 10%.

For high strain rate compression, the comparison between the mesoscale model and a homogeneous FE model clearly demonstrates a significant contribution of the mesoscopic heterogeneity on the overall dynamic increase factor (DIF), suggesting that the experimentally observed bulk DIF is at least partially attributable to the effect of the mesoscale heterogeneity.

The mesoscale modelling framework proves to be robust and reliable in dealing with problems of different complexities in terms of loading condition and nonlinear material responses. The mesoscale model will be extended to investigate the mechanisms governing the concrete behaviour in more general structural settings and involving reinforcement steels. Extension of the framework to 3D models is also currently under way.

Acknowledgements

The research was conducted while Dr. Zhenguo Tu was working at The University of Edinburgh as a post-doctorial research associate.

References

- Agioutantis, Z., Chatzopoulou, E. and Stavroulaki, M. (2000), "A numerical investigation of the effect of the interfacial zone in the concrete mixture under uniaxial compression: the case of the dilute limit", *Cement Concrete Res.*, **30**(7), 715-723.
- ASM (2000), *Metals Handbook*, Vol. 8, Mechanical Testing & Evaluation.
- Bazant, Z.P. and Pfeiffer, P.A. (1987), "Determination of fracture energy from size effect and brittleness number", *ACI Mater. J.*, **84**, 463-480.

- CEB (1993), *CEB-FIP Model Code 1990*, Comité Euro-International du Béton, Redwood Books.
- Dong, A.A., Lu, Y. and Ma, G.W. (2006), "Numerical simulation study of strain rate effect on dynamic behaviour of concrete material", *Proceeding of the Design and Analysis of Protective Structures (DAPS06)*, Singapore, 280-288.
- Eckardt, S., Hafner, S. and Konke, C. (2004), "Simulation of the fracture behaviour of concrete using continuum damage models at the mesoscale", *Proceedings of ECCOMAS*, Jyväskylä.
- Gopalaratnam, V.S. and Shah, S.P. (1985), "Softening response of plain concrete in direct tension", *ACI J.*, **82**(3), 310-323.
- Grote, D.L., Park, S.W. and Zhou, M. (2001), "Dynamic behaviour of concrete at high strain rates and pressures: I. experimental characterization", *Int. J. Impact Eng.*, **25**, 869-886.
- Li, Q.M. and Meng, H. (2003), "About the dynamic strength enhancement of concrete-like materials in a split Hopkinson pressure bar test", *Int. J. Impact Eng.*, **40**, 343-360.
- LS-DYNA (2007), *Keyword User's Manual*, Version 971, Livermore Software Technology Corporation.
- Lu, Y. and Xu, K. (2004), "Modelling of concrete materials under blast loading", *Int. J. Solids Struct.*, **41**(1), 131-143.
- Mindess, S., Young, J.F. and Darwin, D. (2003), *Concrete*, 2nd Edition, Prentice Hall.
- Nagai, K., Sato, Y. and Ueda, T. (2005), "Mesoscopic simulation of failure of mortar and concrete by 3D RBSM", *J. Adv. Concrete Tech.*, **3**(3), 385-402.
- Park, S.W., Xia, Q. and Zhou, M. (2001), "Dynamic behaviour of concrete at high strain rates and pressures: I. numerical simulation", *Int. J. Impact Eng.*, **25**, 887-910.
- Tedesco, J.W., Hughes, M.L. and Ross, C.A. (1994), "Numerical simulation of high strain rate concrete compression tests", *Comput. Struct.*, **51**(1), 65-77.
- Tu, Z.G. and Lu, Y. (2011), "Mesoscale modelling of concrete for static and dynamic response analysis, Part 1: Model development and implementation", *Struct. Eng. Mech.*, **37**(2), 197-213.
- Ueda, M., Hasebe, N. and Sato, M. (1993), "Okuda H. Fracture mechanism of plain concrete under uniaxial tension". *J. Mater. Concrete Struct. Pavements*, **19**, 69-78. (in Japanese)
- van Vliet, M.R.A. and van Mier, J.G.M. (1996), "Experimental investigation of concrete fracture under uniaxial compression", *Mech. Cohes. Fract. Mater.*, **1**, 115-127.
- Zhou, X.Q. and Hao, H. (2008), "Modelling of compressive behaviour of concrete-like materials at high strain rate". *Int. J. Solids Struct.*, **45**, 4648-4661.